

Seismic performance evaluation of coupled core walls with concrete and steel coupling beams

Patrick J. Fortney[†]

Department of Civil Engineering, Clemson University, Clemson, SC 29634, USA

Bahram M. Shahrooz[‡] and Gian A. Rassati^{‡†}

Department of Civil and Environmental Engineering, University of Cincinnati, Cincinnati, OH 45212, USA

(Received January 2, 2007, Accepted May 31, 2007)

Abstract. When coupling beams are proportioned appropriately in coupled core wall (CCW) systems, the input energy from ground motions is dissipated primarily through inelastic deformations in plastic hinge regions at the ends of the coupling beams. It is desirable that the plastic hinges form at the beam ends while the base wall piers remain elastic. The strength and stiffness of the coupling beams are, therefore, crucial if the desired global behavior of the CCW system is to be achieved. This paper presents the results of nonlinear response history analysis of two 20-story CCW buildings. Both buildings have the same geometric dimensions, and the components of the buildings are designed based on the equivalent lateral force procedure. However, one building is fitted with steel coupling beams while the other is fitted with diagonally reinforced concrete coupling beams. The force-deflection relationships of both beams are based on experimental data, while the moment-curvature and axial load-moment relationships of the wall piers are analytically generated from cross-sectional fiber analyses. Using the aforementioned beam and wall properties, nonlinear response history analyses are performed. Superiority of the steel coupling beams is demonstrated through detailed evaluations of local and global responses computed for a number of recorded and artificially generated ground motions.

Keywords: coupled core wall; coupling beam; dynamic analysis; hysteresis; nonlinear analysis; seismic loading; time-history.

1. Introduction

Coupled core wall (CCW) systems have been shown to be excellent lateral force resisting systems. Lateral forces are resisted through a combination of frame action resulting from coupling beam shear forces transferred to wall piers as axial loads, and through flexural deformation of the individual wall piers. The extent of frame action achieved has direct effects on the lateral stiffness of the system. Hence, lateral stiffness is increased as larger shear forces are permitted in the beams and subsequently transferred to the wall piers in the form of axial loads. Therefore, to increase the lateral stiffness of the CCW system, the shear demands on the coupling beams must be increased. However, limited floor-to-

[†]Assistant Professor of Civil Engineering, Corresponding Author, E-mail; pat.fortney@ces.clemson.edu

[‡]Professor of Structural Engineering

^{‡†}Assistant Professor of Civil Engineering

floor-heights in practical CCW buildings may run counter to the expectation of increased coupling beam shear demands depending on the type of coupling beam used.

Diagonally reinforced coupling beams (DCB) have been shown to dissipate large amounts of energy and behave with stable hysteretic response (Paulay 1971, Paulay and Binney 1974). However, the experimental work pertaining to the behavior of DCB's has primarily focused on deep DCB's with span-to-depth ratios of approximately one. Considering that the typical span of a coupling beam is about 1.83 m, the beam would be 1.83 m deep resulting in excessively large floor-to-floor heights. Span-to-depth ratios of coupling beams in practical CCW buildings are between 2 and 4. Hence, practical coupling beam depth for a 1.83 m span would be between 0.92 m and 0.46 m resulting in a much more shallow beam relative to what has been investigated in the past. The large shear demands have raised concerns regarding the behavior of shallow diagonally reinforced coupling beams with span-to-depth ratios between two and four.

The relatively low angle of inclination of the diagonal bar groups in shallow DCB's, combined with large shear demands, presents significant design challenges in that shallow DCB's can be very difficult if not impossible to construct (Harries *et al.* 2005, Fortney 2005). Furthermore, experimental data related to the behavior of shallow DCB's are sparse and deemed inadequate. For these reasons, researchers have endeavored to find legitimate alternatives to the diagonally reinforced coupling beam. One viable alternative to the DCB is a steel coupling beam (SCB). Steel coupling beams have been shown to dissipate a substantial amount of energy, and provide excellent strength and stiffness without requiring large cross-sectional depth (Gong and Shahrooz 2001(a) and 2001(b), Harries *et al.* 1993, Harries *et al.* 1995, Shahrooz *et al.* 1992, Shahrooz *et al.* 1993).

This paper presents the results of nonlinear response history analyses of two twenty-story buildings, each with the same geometric dimensions. One of the two buildings has diagonally reinforced concrete coupling beams and the other one has steel coupling beams (SCB). In both buildings, the span-to-depth ratios of the coupling beams are between two and four. It is important to recognize that large shear demands can be easily achieved with 'shallow' SCB's whereas it is quite difficult with DCB's.

A description of the building geometry is first presented followed by discussion of the design procedures of the two buildings. Key information regarding the experimental procedures used to establish the beams' hysteretic characteristics used in the nonlinear dynamic analyses are presented next, and then followed by other modeling aspects of the two buildings. Finally, performances of the two buildings are compared along with relevant conclusions drawn from the presented results.

2. Elastic analysis and design

The two 20-story buildings, designed using NEHRP 2000 (FEMA 368), are assumed to be located in San Francisco on a Class C (soft rock) site where $S_s = 1.5$ g and $S_1 = 0.65$ g. The site falls into Seismic Use Group 1 and Seismic Design Category D. The buildings have 2.74 m floor-to-floor heights, 178 mm thick post-tensioned floor slabs, and 610 mm thick wall piers. The plan dimensions are 24.4 m by 24.4 m, and the out-to-out core dimensions are 9.1 m by 6 m. Fig. 1 shows a representative floor plan of the two buildings. Floor superimposed dead and live gravity loads are assumed to be 1 kPa and 2.4 kPa, respectively. Cladding dead load is assumed to be 4.4 kN/m and is applied to the exterior edges of the floor plate. The specified strength of all concrete is 35 MPa, 248 MPa steel was used for the steel beams, and 414 MPa reinforcement was used for wall piers and diagonally reinforced concrete beams.

The two buildings were designed using the equivalent lateral force procedure as permitted by FEMA

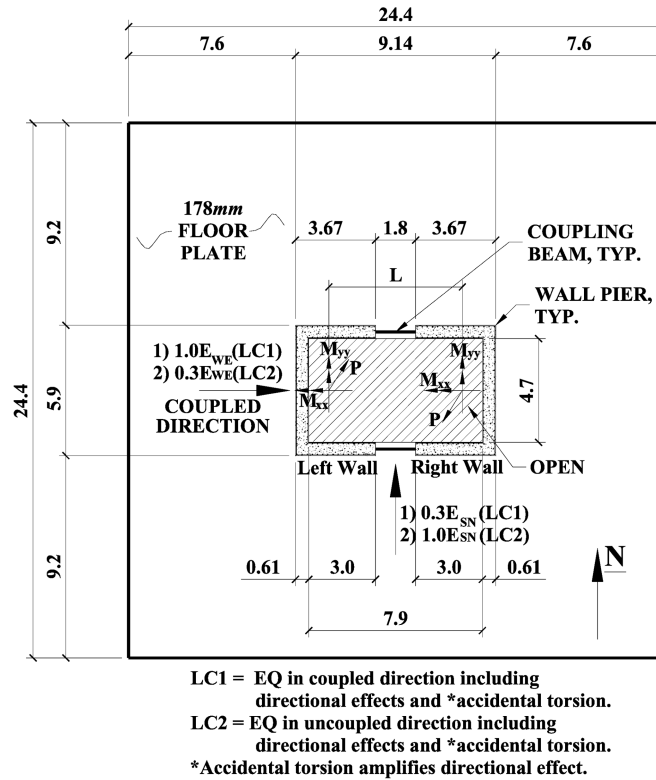


Fig. 1 Floor plan of SCB and DCB buildings with load case (LC) information

368. The calculated weights of the SCB and DCB buildings are 85,099 kN and 85,410 kN, respectively. The seismic coefficient was determined to be 0.0682 resulting in base shears of 5,805 kN and 5,828 kN. The ETABS (Computers and Structures, Inc., v8.4.5) analysis program was used to perform a 3-dimensional elastic analysis of both structures (bidirectional effects were considered). After several iterations of design, analysis, redesign, and reanalysis, a final design of the coupling beams and wall piers was obtained. Tables 1 and 2 show the coupling beams' design shear demands, cross-sectional properties, and design shear capacities. As can be seen in Tables 1 and 2, the beam strengths of the beams were varied over the building height such that the same coupling beam could be used in groups consisting of four floor levels. As a result, floors 1-4, 5-8, 9-12, 13-16, and 17-20 each had beams with different shear strengths. Moreover, the strength of the beams was varied vertically over the building height in an attempt to minimize wall overstrength factors resulting in smaller wall pier design forces (Harries and

Table 1 Cross-sectional properties and capacities of SCB beams in SCB building

Floor levels	d (mm)	h_w (mm)	t_w (mm)	b_f (mm)	t_f (mm)	V_u (kN)	ϕV_n (kN)	$V_u/\phi V_n$
17-20	419	318	13	330	51	445	540	0.82
13-16	419	318	19	330	51	753	811	0.93
9-12	419	318	25	330	51	1032	1081	0.95
5-8	419	318	27	330	51	1109	1151	0.96
1-4	419	318	25	330	51	995	1081	0.92

See list of symbols for definitions of symbols in table

Table 2 Cross-sectional properties and capacities of DCB beams in DCB building

Floor levels	b_w (mm)	h (mm)	d_w (mm)	d_h (mm)	V_u (kN)	ϕV_n (kN)	$V_u/\phi V_n$
20-17	610	457	305	127	285	330	0.86
13-16	610	457	330	203	480	483	0.99
9-12	610	508	305	229	677	707	0.96
5-8	610	610	305	279	1096	1119	0.98
1-4	610	559	305	254	745	757	0.98

See list of symbols for definitions of symbols in table

McNiece 2005, Fortney 2005).

Well established design methodologies, from past research, was used to design the steel coupling beams (SCB) in the SCB building. Fortney *et al.* 2006(a) provides a detailed description of the design procedures for steel coupling beams. The diagonally reinforced concrete coupling beams (DCB) in the DCB building were designed such that the shear strengths of the beams satisfied ACI 318 (Building Code Requirements for Structural Concrete) provisions. However, in order to reduce the steel congestion common to diagonally reinforced coupling beams, various ACI 318 transverse reinforcement spacing requirements were not satisfied. An effective moment of inertia recommended by Paulay and Priestley (1992) was used in the elastic analysis for the DCB's in the DCB building (Levels 13-20: $1.935 \times 10^9 \text{ mm}^4$; 9-12: $2.163 \times 10^9 \text{ mm}^4$; 5-8: $3.542 \times 10^9 \text{ mm}^4$; 1-4: $2.770 \times 10^9 \text{ mm}^4$). A detailed discussion on the design of the DCB is presented in Fortney *et al.* 2006(b). The cross-sectional dimensions of the DCB's and their associated design capacities are given in Table 2.

It has been shown that there exists a class of CCW systems where the concrete compressive strains in the wall piers are moderate enough that special boundary elements are not required in the wall piers (Fortney *et al.* 2006(c)). With this in mind, the wall piers were designed with one curtain of uniformly distributed longitudinal reinforcement at each exterior face. To account for cracked sections for the wall piers, the elastic modulus of the wall pier concrete was factored as recommended by ACI 318 Section 10.11.1 ($0.70 E I_g$ for wall piers above the first floor, and $0.35 E I_g$ for the base wall piers). To ensure plastic hinge formation in the coupling beams prior to base wall pier hinging, a wall overstrength factor (the ratio of the sum of the nominal coupling beam shear capacities to the sum of the factored coupling beam shear demands) was applied to the elastic design forces. The design wall pier demands are multiplied by the wall overstrength factor, which is greater than 1.0, to ensure that the wall piers remain elastic up to a level of loading that would cause all of the coupling beams to reach their nominal shear capacities (Harries and McNiece 2005, Fortney 2005). As will be discussed later in this document the wall overstrength factors, at the base of the walls, for the SCB and DBCB buildings were 1.62 and 2.12, respectively. Although a wall overstrength factor is not required by American codes, the authors recommend the application of the wall overstrength factor in an elastic strength-based design to ensure the desired global behavior of the CCW system. In both buildings, the final wall pier designs resulted in different cross-sectional designs at floors 1-4, 5-8, and 9-20. The wall pier reinforcement for both buildings is summarized in Table 3.

Two earthquake load cases were considered. Load case one (LC1) considers an earthquake acting West-to-East where 100% of the earthquake loads are applied in the West-East direction with 30% of the earthquake loads applied in the South-North direction. Load case two (LC2) considers an earthquake acting South-North where 100% of the earthquake loads are applied in the South-North direction with 30% of the earthquake loads acting in the West-East direction. In both cases, accidental torsion is considered

Table 3 Wall pier reinforcement in the SCB and DCB buildings

Structure	Floors	(%)	Bar qty.	Bar size (#)	Bar spacing (mm)
SCB	17-20	0.81	92	9	229
	13-16	0.81	92	9	229
	9-12	0.81	92	9	229
	5-8	1.26	92	11	229
	1-4	1.82	92	14	229
DCB	17-20	1.04	118	9	205
	13-16	1.04	118	9	205
	9-12	1.04	118	9	205
	5-8	1.31	118	10	205
	1-4	2.33	118	14	205

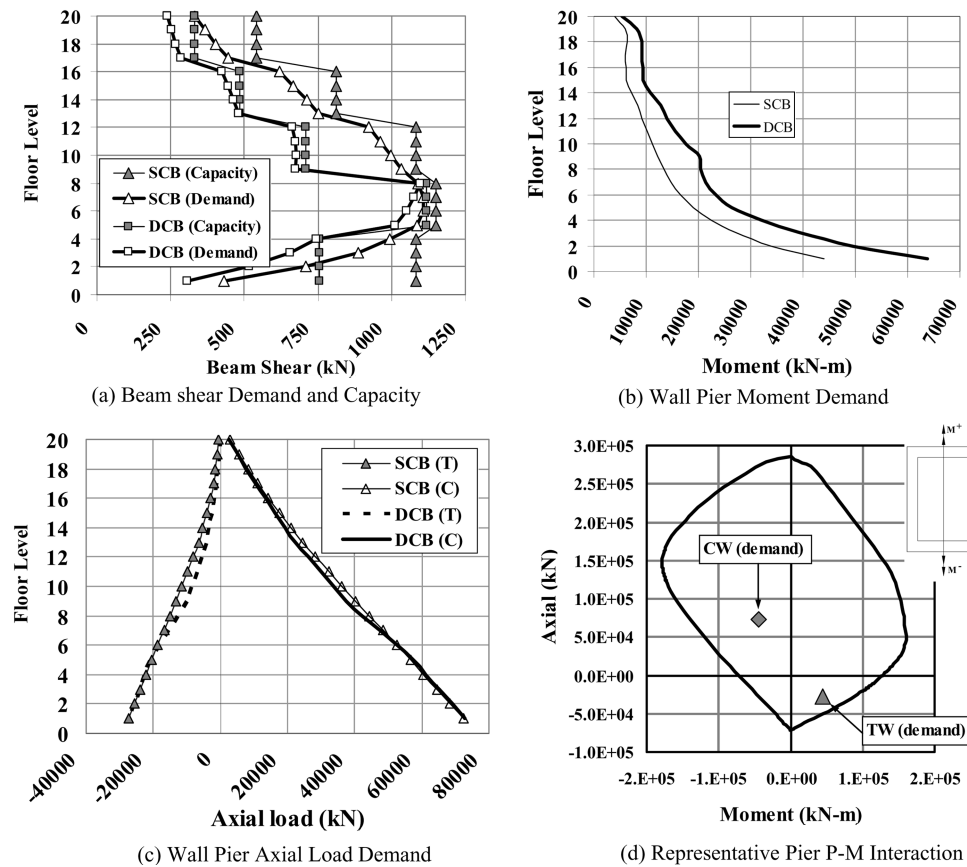


Fig. 2 Demands and capacities from ELF elastic analysis. The P-M interaction shown in part

and is applied so as to increase the impact of bi-directional effects. See Fig. 1 for the loading directions. Fig. 2(a) shows the beam shear demands and capacities, wall pier moments, axial load demands, and a representative P-M interaction diagram for the wall piers, for both buildings. Refer to Fortney (2005) for a detailed discussion regarding the elastic analysis and design of the two buildings. The final

designs of the SCB and DCB buildings resulted in degrees of coupling (DOC) (see Equation 1) of 72% and 67%, respectively.

$$DOC = \frac{(\sum V_n)L}{(\sum V_n)L + M_T} \tag{1}$$

3. Experimental program

One-half scale SCB and DCB coupling beam-wall pier subassemblies were tested with increasing cycles of force/displacement applied in a reverse cyclic fashion. Fig. 3 shows a photo of the test setup with a specimen installed and a representative load history. A detailed discussion pertaining to the experimental testing can be found in Fortney *et al.* (2006(a)) and Fortney *et al.* (2006(b)). A sufficient

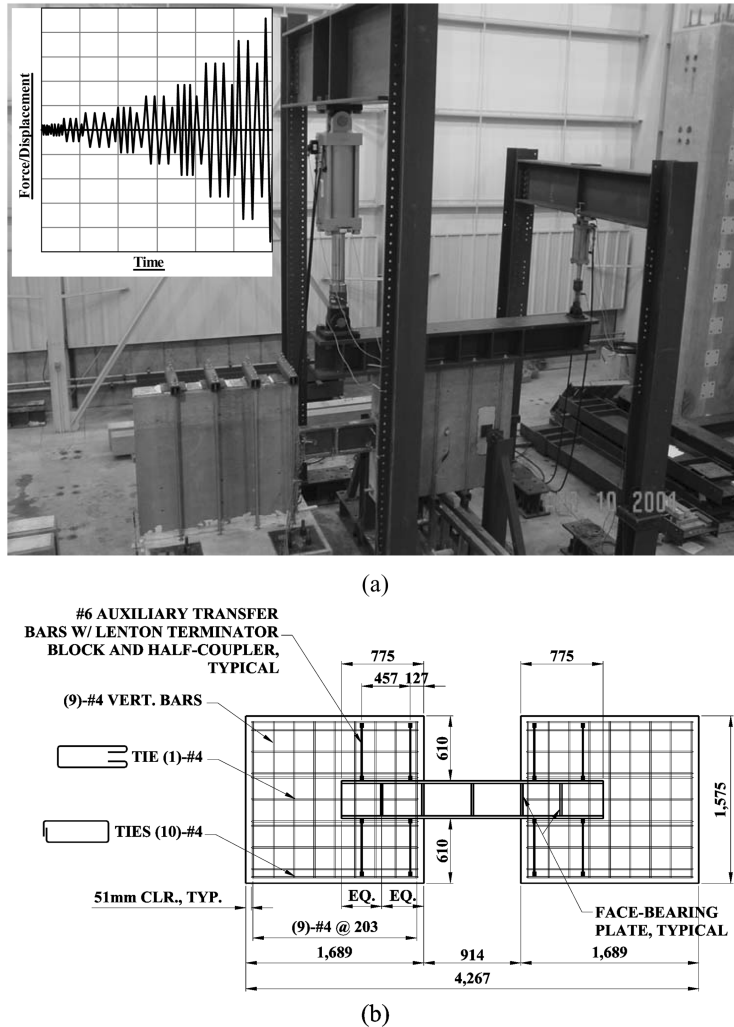


Fig. 3 (a) Photo of test setup and representative reverse cyclic load history; (b) schematic of SCB specimen (DCB specimen had like wall geometry)

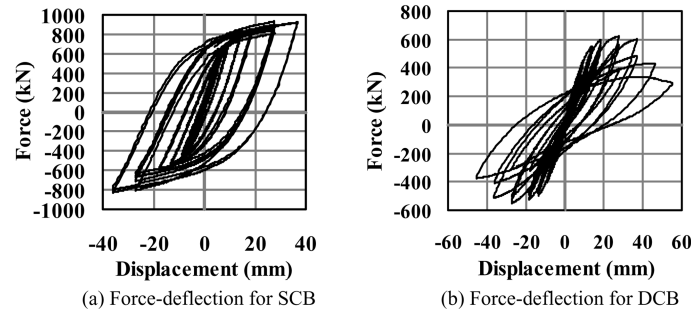


Fig. 4 Force deflection for (a) SCB and (b) DCB

number of strain gages, displacement transducers, and tilt meters were used to capture critical responses. Force–displacement relationships were generated from the measured data. Figs. 4(a) and 4(b) show the measured force-displacement relationships of the SCB and DCB, respectively.

4. Nonlinear modeling and analysis

4.1 Beam hysteretic models

The experimentally measured hysteretic characteristics were used to identify the model parameters for simulating the behavior of the coupling beams in the nonlinear analyses. To facilitate this process, the Hysteresis module of the Ruaumoko Nonlinear Analysis program (University of Canterbury, v2.6) was used. The Hysteresis module uses known mathematical hysteresis rules to “match” measured hysteretic behavior. The procedure is an iterative process where the hysteresis rule parameters are adjusted until the mathematical model generates a force-deflection ($F-d$) relationship that correlates with a given $F-d$ curve which in this case was the experimentally measured responses shown in Figs. 4(a) and 4(b).

Fig. 5(a) shows correlation of the Al-Bermani mathematical model used for the SCB against the measured response; and Fig. 5(b) compares analytically generated $F-d$ responses, as computed by Modified Takeda model, against its experimental counterpart for the SCB. Tables 4 and 5 show the

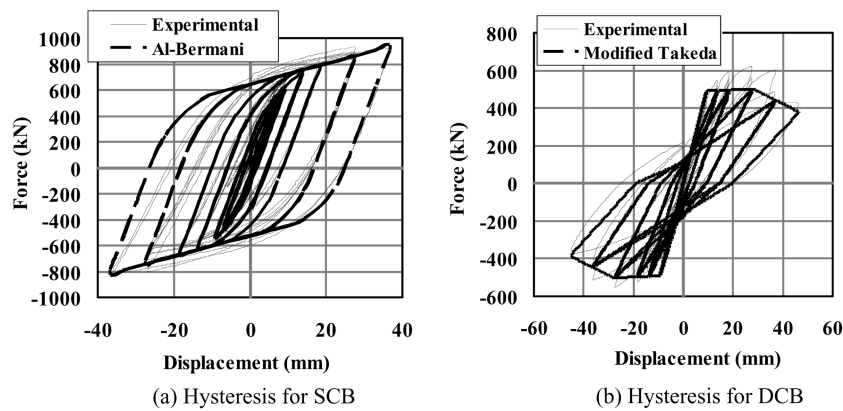


Fig. 5 Hysteretic models for (a) SCB and (b) DCB

parameters used for each hysteresis model to achieve the correlations shown in Fig. 5. Note that the Al-Bermani model correlates very well with the experimentally measured hysteresis of the SCB however, the Modified Takeda model does not correlate as well with the DCB. The Modified Takeda model shown in Fig. 5(b) is the best correlation that could be achieved. Further increases or decreases in the Modified Takeda strength degradation parameters resulted in undesirable shifts in the individual hysteretic peak coordinates.

4.2 Scaled hysteresis

The aforementioned hysteresis parameters were based on the experimental data from a 1/2 scale model of the beams in the 20-story buildings. Therefore, the initial stiffness, positive yield force, and negative yield force must be scaled for the full-scale beams. Accordingly, initial stiffness, k_0 , has to be multiplied by 2, and the yield strengths (F_y^+ and F_y^-) have to be multiplied by 4. Additional adjustments are needed to account for the different size beams, which do not correspond to full-scale equivalent of the test specimens, used over the height of the buildings. The shear capacity of a SCB is directly proportional to the area of the web. Therefore, the scaling factor is the ratio of the web area of a full-scale equivalent of the test beams (which were the basis of the identified parameters shown in Table 4) to the web area of a particular beam at a given floor level. The web area of the experimental beam is $4,516 \text{ mm}^2$; hence, the web area of the equivalent full-scale beam is $(4)(4,516 \text{ mm}^2) = 18,064 \text{ mm}^2$. The web area of the beams at floor levels 1-4 is $8,065 \text{ mm}^2$. Therefore, the full-scale hysteretic parameters, for beams at floor levels 1-4, are scaled by a factor of $8,065/18,064=0.4465$, resulting in values of $k_0 = (79)(2)(0.4465) = 70 \text{ kN/m}$, $F_y^{(+)} = (712)(4)(0.4465) = 1,271 \text{ kN}$, and $F_y^{(-)} = (-578)(4)(0.4465) = -1,033 \text{ kN}$. The parameters of the beams at the other floor levels are scaled in the same manner.

To account for scaling of the hysteretic parameters for the diagonally reinforced beams, a similar procedure was used as that described for the SCB. However, the shear strength of a diagonally-reinforced concrete beam is directly proportional to $A_{vd}\sin\alpha$ where A_{vd} is the steel area of one diagonal bar group and α is the angle of inclination of the diagonal bar group. For example, $A_{vd}\sin\alpha$ for the experimental beam is 562 mm^2 ; hence, for a full-scale beam, $A_{vd}\sin\alpha = (4)(562 \text{ mm}^2) = 2,248 \text{ mm}^2$.

Table 4 Hysteresis parameters for SCB

Al-Bermani hysteresis model - hysteresis parameters for SCB					
Initial stiffness, Yield and bilinear factor				Strength degradation	
k_0 (kN/mm)	$F_y^{(+)}$ (kN)	$F_y^{(-)}$ (kN)	r	α	β
79	712	-578	0.1	0.2	0.2

Table 5 Hysteresis parameters for DCB

Modified Takeda hysteresis model - hysteretic parameters for DCB					
Initial stiffness, Yield and bilinear factor				Power factor and unloading	
k_0 (kN/mm)	r	F_y^+ (kN)	F_y^- (kN)	Power factor N	unload a_s
53	0.01	489	-489	1	1
Strength degradation					
Ductility at start	Ductility at final	Final strength equal to 0.01	α	β	
3	6.52	7.52	0.5	0.001	

The value $A_{v,d}\sin\alpha$ for the beams at floor levels 1-4 is 1,219 mm². Therefore, the hysteretic parameters for the beams at floor levels 1-4 are scaled by $(1,219/2,248) = 0.5423$. Thus, the hysteretic parameters for the beams at floor levels 1-4 are $k_0 = (57)(2)(0.5423) = 57$ kN/m, $F_y^{(+)} = (489)(4)(0.5423) = 1,062$ kN, and $F_y^{(-)} = (-489)(4)(0.5423) = -1,062$ kN. The beams at the other floor levels are scaled similarly.

4.3 Wall pier properties

To determine the wall pier properties in the analytical model, axial force-moment interaction (P-M) diagrams were generated. In generating the P-M diagrams, the limiting concrete compressive strain and steel tension strains were taken as 0.003 and 0.15, respectively. Thus, the P-M diagrams represent failure surfaces considering these strains. In the following discussions, the term ‘failure’ implies a combination of axial force and moment that falls outside of the P-M surface which was generated based on these aforementioned strains. $M-\phi$ diagrams were used to determine the effective moments of inertia and bilinear factors. For both buildings, the design of the longitudinal steel for the wall piers in floor levels 9-20 are the same. The longitudinal steel is different for floor levels 5-8 and 1-4. Thus, different wall pier properties were determined for floor levels 1-4, 5-8, and 9-20. Additionally, to account for hinging at the base of the wall piers, the parameters used to define the base wall pier (level 1), are different than the parameters used for the wall piers at floor levels 2-4.

The reported nonlinear analyses are in the coupled direction (see Fig. 1). In this direction, the C-shape walls do not have symmetrical P-M interaction diagrams. A larger moment capacity is achieved when the web is in compression (negative moment) than when the web is in tension (positive moment). The critical points used to define the P-M diagrams for the different wall piers are shown in the supporting schematic beneath Table 6 (which summarizes the wall pier P-M parameters). A fiber cross-sectional

Table 6 Wall pier P-M parameters

Quadratic beam-column yield surface parameters - wall piers						
Floor Levels	PYC (kN)	P (PB) (kN)	B (MB) (kN-m)	C (PC) (kN)	C (MC) (kN-m)	PYT (kN)
SCB model						
L1-4	-285,784	-152,566	178,146	-46,526	-160,114	67,788
L5-8	-279,290	-149,408	149,946	-67,876	-136,795	38,177
L9-20	-271,461	-150,476	141,811	-86,336	-131,277	29,370
DBC model						
L1-4	-291,566	-148,430	165,673	-54,844	-146,421	34,565
L5-8	-277,155	-145,894	150,082	-82,866	-135,711	34,428
L9-20	-265,546	-143,893	137,337	-92,696	-127,346	22,075

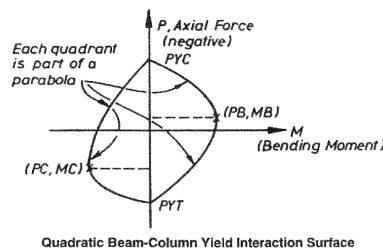


(figure from Ruaumoko Nonlinear program Users' Manual; NOTE that Ruaumoko's model assumes tension to be positive)

analysis application, XTRACT (Imbsen) was used to generate P-M interaction diagrams (as well as $M-\phi$ relationships as discussed in following paragraph).

The asymmetric behavior of C-shape walls also has a direct influence on the moment-curvature relationships of the wall. The positive moment-curvature relationship is much softer than the negative moment-curvature relationship. Load reversals during a seismic event will subject wall piers to positive and negative moments, i.e., a wall pier will act as a tension wall or a compression wall depending on the direction of loading. However, the Modified Takeda hysteresis, as implemented in Ruaumoko, does not allow unsymmetrical properties, and only one set of parameters can be input to define the wall piers. The elastic and inelastic stiffness properties for the tension wall and compression wall moment-curvatures were averaged to overcome the limitations of Ruaumoko. It is important to note that this

Table 7 Elastic and inelastic EI slopes for all wall piers in the SCB building

Elastic moment-curvature slopes – SCB model							
Wall gross moment of inertia (considering steel)				Average moment of inertia			
Floor levels	$E_{c,wall}$ (kN/m ²)	I_g (m ⁴)	EI_g (kN-m ²)	EI (CW) (kN-m ²)	EI (TW) (kN-m ²)	EI (AVG) (kN-m ²)	I_{AVG} (m ⁴)
L1-4	27,787,983	9.26	257,345,510	169,425,366	46,488,668	107,957,017	3.89
L5-8	27,787,983	9.21	255,906,486	139,428,114	25,779,719	82,603,917	2.97
L9-20	27,787,983	9.16	254,467,462	105,309,021	20,475,489	62,892,255	2.26

Wall pier yield coordinates for SCB model						
Floor levels	Compression wall		Tension wall		Level 1 wall pier	
	M_y (kN-m)	ϕ_y (1/m)	M_y (kN-m)	ϕ_y (1/m)	EI_y (AVG) (kN-m ²)	EI_y (AVG)/ EI_g
L1-4	111,172	0.000656	45,757	0.000984	107,957,017	0.420
L5-8	93,547	0.000671	31,946	0.001239		
L9-20	67,788	0.000644	22,370	0.001093		

Wall moment of inertia			
L1	L2-4	L5-8	L9-20
I_e (m ⁴)			
1.63	3.89	2.97	2.26

Inelastic moment-curvature slopes - SCB model							
Floor Levels	Compression wall		Tension wall		Average of CW and TW		$EI_{SH,AVG} \Delta M_{AVG} / \Delta \phi_{AVG}$ (kN-m ²)
	ΔM (kN-m)	$\Delta \phi$ (1/m)	ΔM (kN-m)	$\Delta \phi$ (1/m)	ΔM_{AVG} (kN-m)	$\Delta \phi_{AVG}$ (1/m)	
L1-4	23,102	0.00414	9,748	0.00310	16,425	0.003622	4534704
L5-8	10,331	0.00757	4,077	0.00783	7,204	0.007698	935739
L9-20	6,792	0.01048	0	0.02553	3,396	0.018005	188620

Bilinear factors		
Floor levels	EI_g (kip-ft ²)	$EI_g/EI_{SH,AVG}$
L1-4	257,345,510	0.0176
L5-8	255,906,486	0.0037
L9-20	254,467,462	0.0007

method will underestimate and overestimate the load-carrying capacity of the compression wall and tension wall, respectively. The axial force used to generate the $M-\phi$ for wall piers 1-4 is the design axial force calculated at level 1. The axial force used to generate the $M-\phi$ for wall piers 5-8 is the design axial force calculated at level 5. Likewise, the design axial force calculated at level 9 was used to generate the $M-\phi$ for wall piers 9-20. The values used in the SCB and DCB buildings to define the wall pier moment-curvature relationships in the nonlinear models are shown in Tables 7 and 8, respectively. Eq. (2) was used to calculate the $E_c J_{y,avg}$ values shown in Tables 7 and 8, which are the averages of the elastic slopes of the bilinear $M-\phi$ relationships of the tension wall and compression wall at a particular level.

Table 8 Elastic and inelastic EI slopes for all wall piers of the DCB building

Elastic moment-curvature slopes – DCB model							
Wall gross moment of inertia (considering steel)				Average moment of inertia			
Floor levels	$E_{c,wall}$ (kN/m ²)	I_g (m ⁴)	EI_g (kN-m ²)	EI (CW) (kN-m ²)	EI (TW) (kN-m ²)	EI (AVG) (kN-m ²)	I_{AVG} (m ⁴)
L1-4	27,787,983	9.56	265,739,819	176,833,770	76,087,272	126,460,521	4.55
L5-8	27,787,983	9.36	259,983,722	188,906,331	33,567,914	111,237,123	4.00
L9-20	27,787,983	9.30	258,304,860	107,612,656	41,587,306	74,599,981	2.68

Wall pier yield coordinates for DCB model						
Floor levels	Compression wall		Tension wall		Level 1 Wall pier	
	M_y (kN-m)	ϕ_y (1/m)	M_y (kN-m)	ϕ_y (1/m)	EI_y (AVG) (kN-m ²)	EI_y (AVG)/ EI_g
L1-4	128,796	0.000728	78,634	0.001033	126,460,521	0.476
L5-8	86,768	0.000459	39,317	0.001171		
L9-20	67,788	0.000630	42,706	0.001027		

Wall moment of inertia			
L1	L2-4	L5-8	L9-20
I_e (m ⁴)			
2.17	4.55	4.00	2.68

Inelastic moment-curvature slopes - DCB model							
Floor levels	Compression wall		Tension wall		Average of CW and TW		$EI_{SH,AVG} \Delta M_{AVG} / \Delta \phi_{AVG}$ (kN-m ²)
	ΔM (kN-m)	$\Delta \phi$ (1/m)	ΔM (kN-m)	$\Delta \phi$ (1/m)	ΔM_{AVG} (kN-m)	$\Delta \phi_{AVG}$ (1/m)	
L1-4	14,371	0.00467	10,222	0.00365	12,297	0.00416	2957018
L5-8	15,035	0.00638	3,430	0.00700	9,233	0.00669	1380144
L9-20	10,331	0.01332	4,379	0.00583	7,355	0.00958	767998

Bilinear factors		
Floor levels	EI_g (kip-ft ²)	$EI_g/EI_{SH,AVG}$
L1-4	265,739,819	0.0111
L5-8	259,983,722	0.0053
L9-20	258,304,860	0.0030

$$E_c I_{y,AVG} = \frac{E_c I_y(TW) + E_c I_y(CW)}{2} = \frac{\frac{M_{y,TW}}{\phi_{y,TW}} + \frac{M_{y,CW}}{\phi_{y,CW}}}{2} \quad (2)$$

The effective moments of inertia (I_e) for the wall piers were calculated as shown in Eq. (3).

$$I_e = \frac{E_c I_{y,AVG}}{E_c} \quad (3)$$

The moments of inertia for the base wall piers, $I_{e,base}$, were taken as the average of the ratios of EI_y/EI_g for the tension wall and compression wall times I_e , as shown in Eq. (4).

$$I_{e,base} = \left[\frac{\left(\frac{E_c I_y(TW)}{E_c I_g} + \frac{E_c I_y(CW)}{E_c I_g} \right)}{2} \right] I_e \quad (4)$$

To determine the bilinear factor (i.e. the parameter that defines the behavior of the wall beyond the yield point), the average of the post-peak slopes (EI_{SH}) of the tension wall and compression wall moment-curvatures was used. Equation 5 shows how the bilinear factor, r , was computed. In Equation 5, ΔM and $\Delta \phi$ define the slopes of the post yield bilinear $M-\phi$ curves.

$$r = \frac{\frac{E_c I_{SH}(TW)}{E_c I_g} + \frac{E_c I_{SH}(CW)}{E_c I_g}}{2} = \frac{\frac{\Delta M_{TW}}{\Delta \phi_{TW}} + \frac{\Delta M_{CW}}{\Delta \phi_{CW}}}{2} \quad (5)$$

4.4 Model

The cores of the buildings were modeled as 2-D equivalent frames where the “columns” of the frame have the properties of the wall piers and are located at the centroids of the wall piers. Fig. 6 shows the plan dimensions of the core, where the centroids of the walls are located, and a partial elevation of the equivalent frame.

The wall piers were modeled as general quadratic beam-column frame members. The Modified Takeda hysteresis rule was used to define the wall pier response, and hysteretic strength degradation in each direction was considered to be based on ductility. The Modified Takeda and hysteretic strength reduction parameters were determined based on engineering judgment, and previous experience with modeling of walls. While determining the parameters for hysteretic strength reduction, the fact that the wall pier concrete is unconfined (no boundary elements) was taken into account. The modified Takeda parameters for the wall piers are $\alpha = 0$ and $\beta = 0.6$. Fig. 7 shows the hysteretic strength reduction used for the wall piers.

The measured force-deflection curves for the experimental beams were generated based on transverse forces imparted to the beams, and these curves represent combined effects of shear, flexure, and level of beam/wall pier fixity. The yield forces assigned to Ruaumoko beam members represent yield forces associated with flexural hinging which is not representative of the measured F-d curve. For this reason, the coupling beams were modeled as spring elements (see Fig. 6). The spring element consists of a

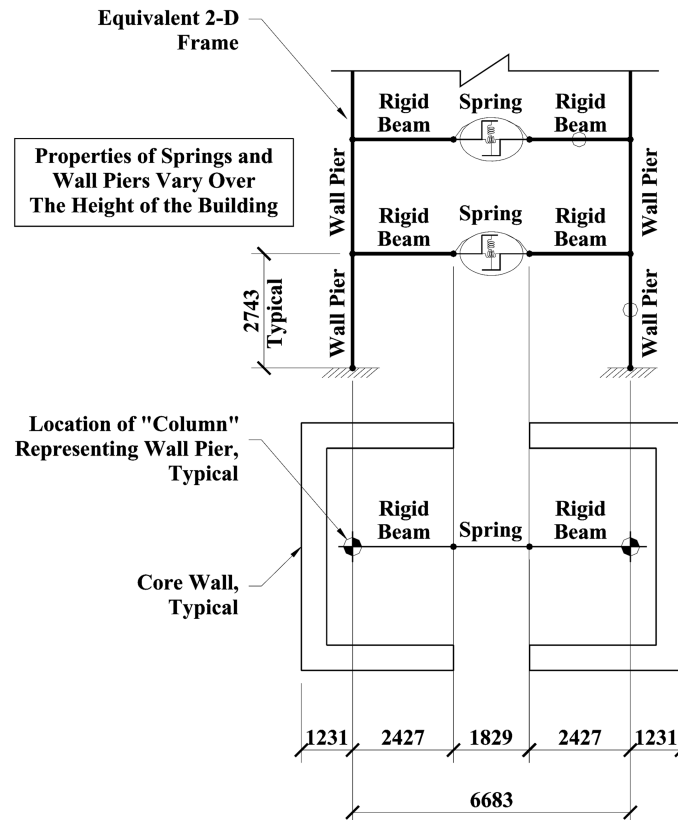


Fig. 6 Plan and partial elevation of nonlinear model

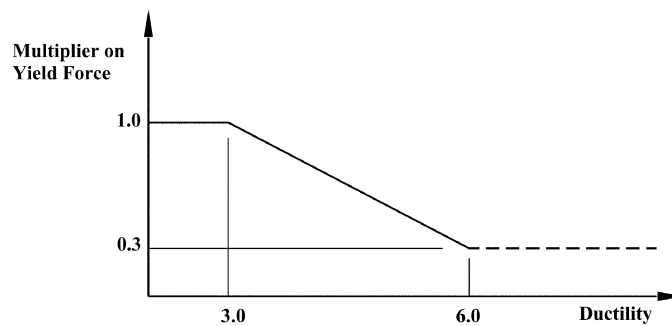
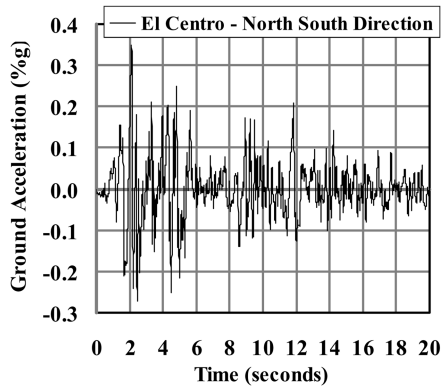


Fig. 7 Strength degradation rule for wall piers

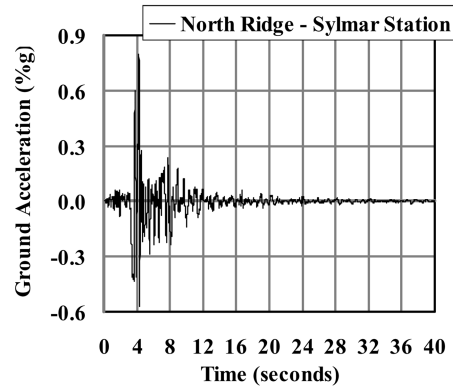
longitudinal, rotational, and transverse spring. The spring is modeled to have no interaction between the longitudinal, rotational, and transverse spring components. Sufficiently large stiffness and yield forces are assigned to the longitudinal and rotational springs to ensure rigid behavior. The hysteretic parameters determined for the steel and diagonally-reinforced coupling beams are assigned to the transverse spring. Thus, transverse loading governs the hysteretic behavior of the coupling beams. Table 9 shows the spring element parameters for both buildings for floor levels 1-4, 5-8, 9-12, 13-16, and 17-20, respectively (note that the tabulated beam parameters account for having two coupling beams in the equivalent

Table 9 Spring properties used for coupling beams in nonlinear model

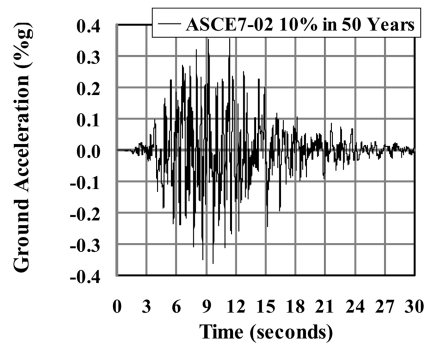
Floor level	Model	F_{y^+} (kN)	F_{y^-} (kN)	k_0^- (kN/mm)	r	α	β
Floors 1-4	SCB	2542	-2066	140	0.10	0.20	0.200
	DCB	2124	-2144	114	0.01	0.50	0.001
Floors 5-8	SCB	2706	-2200	150	0.10	0.20	0.200
	DCB	3142	-3142	168	0.01	0.50	0.001
Floors 9-12	SCB	2542	-2066	140	0.10	0.20	0.200
	DCB	1984	-1984	106	0.01	0.50	0.001
Floors 13-16	SCB	1906	-1548	106	0.10	0.20	0.200
	DCB	946	-946	50	0.01	0.50	0.001
Floors 1-20	SCB	1270	-1032	70	0.10	0.20	0.200
	DCB	928	-928	50	0.01	0.50	0.001



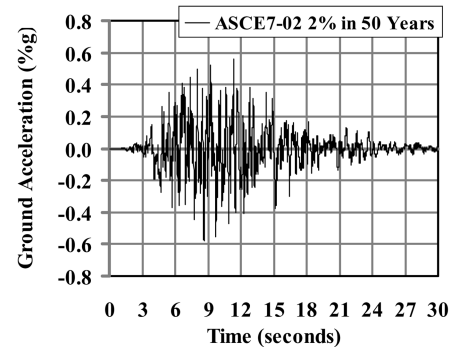
(a) Ground Motion El Centro



(b) Ground Motion Northridge



(c) Ground Motion ASCE 7 – 10% in 50 years



(d) Ground Motion ASCE 7 – 2% in 50 years

Fig. 8 Input ground motions

frame). The rigid links on both sides of the coupling beam connecting the beams to the wall piers are modeled as sufficiently rigid beam-column frame members.

The dynamic weight of the structure was input as dynamic loads assigned to the nodes of the wall piers at each floor level. To distribute the dynamic weight of the structure, the total weight of

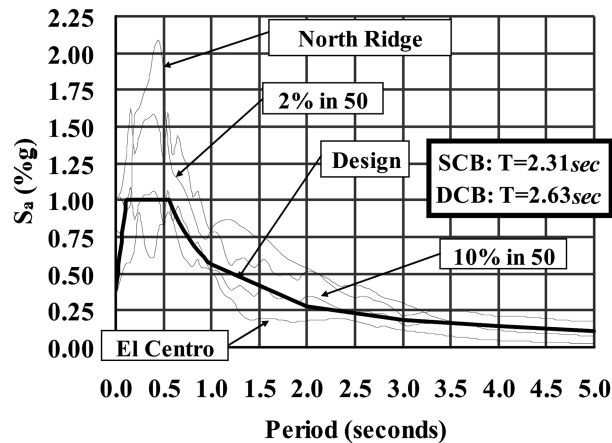


Fig. 9 Spectra for motions shown in Figure 8

the building was distributed evenly over the 20 floor levels. Both the left and right wall piers each were assigned one-half of the dynamic weight in each floor level. The dynamic weights assigned to each wall pier at each floor were 2,126 kN and 2,135 kN for the SCB and DCB buildings, respectively.

A static analysis of the gravity loads is performed prior to the time-history analysis so that residual forces due to gravity loads are considered in the solution of the nonlinear analysis. The gravity loads are assigned to the nodes of the wall piers at each floor level and represent the tributary gravity loads that each wall pier will have at each floor level. The static loads assigned to the node at each wall pier at each floor level are 1,343 kN and 1,481 kN for the SCB and DCB buildings, respectively.

4.5 Nonlinear analysis

Each building was subjected to four different ground motions: (1) the 1940 North-South El Centro ground motion, (2) the 1994 North-South Northridge ground motion, (3) an artificial ground motion representing an ASCE7-02 10% chance of exceedence in 50 years ground motion, and (4) an artificial ground motion representing an ASCE7-02 2% exceedence in 50 years ground motion. The input excitations are shown in Fig. 8. The acceleration spectra for these ground motions are provided in Fig. 9.

The analyses were based on Newmark inelastic dynamic time-history analyses with diagonal mass matrix mass models. The damping model chosen for the time-history analyses is the Rayleigh initial stiffness model, and 5% damping was assumed for both models. Small displacements were considered with simplified P-delta effects.

5. Analyses results

5.1 Base shear

As can be seen in Table 10, the base shears used in the elastic designs were exceeded in the time-history analyses of all four ground motions. The Northridge record produced base shears as much as 3.4

Table 10 Base shears from elastic analysis and nonlinear time-history analysis

$V_{b,ELF}$ (SCB)	Base shears							
5805	El Centro		Northridge		ASCE 7 (10%)		ASCE 7 (2%)	
$V_{b,ELF}$ (DCB)	SCB (kN)	DCB (kN)	SCB (kN)	DCB (kN)	SCB (kN)	DCB (kN)	SCB (kN)	DCB (kN)
5827								
$V_{b,max}$	8229	8674	18148	19660	10853	12188	15479	17169
$V_{b,max}/V_{b,ELF}$	1.4	1.5	3.1	3.4	1.9	2.1	2.7	2.9

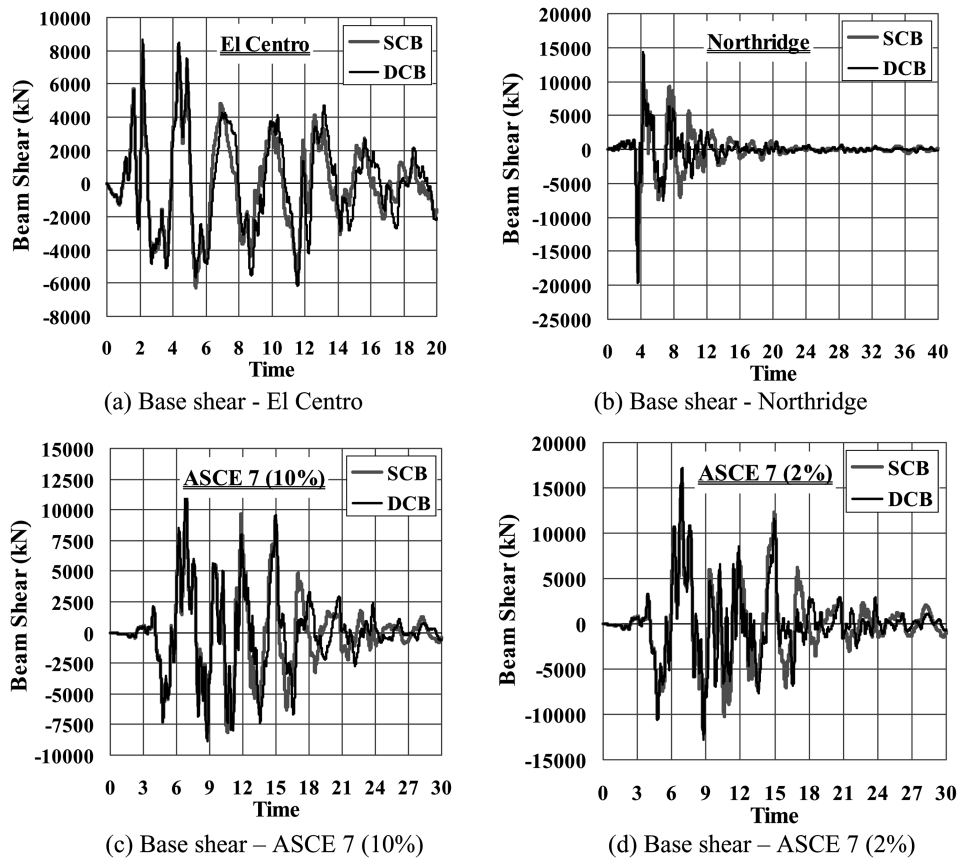


Fig. 10 Base shear history for SCB and DCB buildings. See Table 10 for design base shears from Equivalent Lateral Force procedure.

times the code specified value in the equivalent lateral force (ELF) analysis; the ELF base shears approximated the base shears seen during the El Centro record the closest where the time-history base shears were as little as 1.4 or 1.5 times those from the ELF procedure. As can be seen in Fig. 9, the design response spectrum for the two buildings is a good approximation of the ASCE 7 (10%) artificial record. However, the base shears generated during the ASCE 7 (10%) record produced base shears approximately two times those from the ELF procedure. Fig. 10 shows the base shear histories generated for all four ground motions for both buildings.

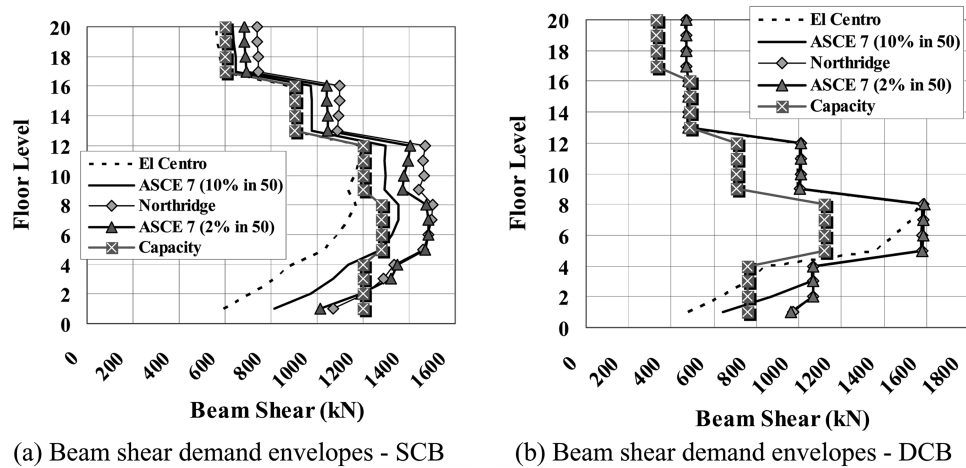


Fig. 11 Envelopes of coupling beam shear demand from four ground motions

5.2 Coupling beam shear demand

Figs. 11(a) and 11(b) show the beams’ shear demand envelopes throughout the history of all four ground motions. As can be seen in the figures, the majority of the coupling beams in the SCB building exceed their capacities during the Northridge and ASCE 7 (10% and 2%) ground motions. However, only the coupling beams in the top eight floors exceed their capacities during the El Centro record. The same trend is seen in Fig. 12(b) for the coupling beams in the DCB building. However, it should be noted that due to the lower DOC of the DCB building relative to the SCB building, the shear demand is relatively larger than the shear capacity compared to the SCB building.

5.3 Wall pier demands

Figs. 12 and 13 show the demand histories of the base wall piers in the SCB and DCB buildings, respectively. The traces of the demands are plotted in the bottom portions of the axial load-moment (P-M) interaction curves generated for the wall piers. As can be seen in both figures, there are no excursions outside of the surfaces defined by the P-M interactions. The same is true for the rest of the wall piers in both buildings. The primary observation to be made in regard to the good performance of the wall piers is that had the wall pier design loads resulting from an elastic analysis not been factored by the wall overstrength factors, the demands obtained from the nonlinear analyses would have exceeded the wall pier capacities. To illustrate this point, the base wall pier design loads including the wall overstrength factors (obtained from the elastic analyses) are plotted in Figs. 12(a) through 12(d) and are compared to the demands observed in the nonlinear analyses. As can be seen in the figures, the wall pier demands determined from the ELF procedure, and then factored by an appropriate wall overstrength factor, give a relatively good approximation of the wall pier demands resulting from nonlinear analyses.

As discussed previously, the desired behavior of a coupled core wall system is that the coupling beams hinge prior to hinge formation in the wall piers. Referring back to Figs. 11(a) and 11(b), it is seen that the majority of the coupling beams over the height of both buildings yielded during the Northridge

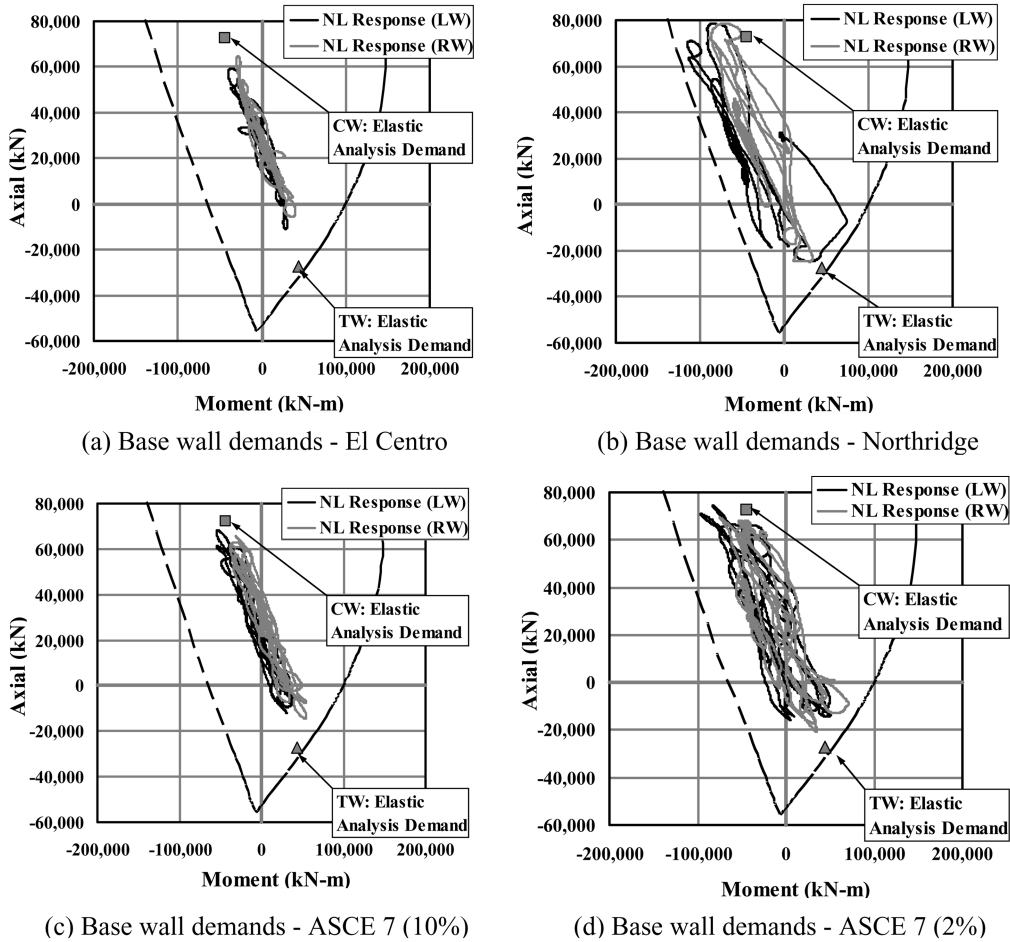


Fig. 12 Trace of base wall pier demand history for the SCB building. CW and TW are abbreviations for compression wall and tension wall, respectively. NL Response is trace of wall pier nonlinear response. (LW) and (RW) are abbreviations for Left Wall and Right Wall, respectively as shown in Figure 1.

and ASCE 7 (10% and 2%) ground motions. The wall piers in the DCB building did not yield during any of the four of the histories indicating that the intended behavior of the system is achieved. The wall piers in the SCB building did not yield during the El Centro and ASCE 7 (10%) ground motions. Only the base wall piers yielded during the Northridge and ASCE 7 (2%) ground motions. First yield in the base wall piers in the SCB building occurred at approximately 7.45 s into the Northridge record. As can be seen in Fig. 14(a), which shows the envelope of the coupling beam shear demands up to the point where the first yield in the wall piers occurred, all but the first two floor coupling beams of the SCB building have already yielded. Similarly, with the exception of the first two floors all the coupling beams over the height of the SCB building had yielded prior to formation of the first yield of the base wall piers in the SCB building during the ASCE 7 (2%) record (Fig. 14b).

In both buildings, the desired beam hinging occurred while the wall piers remained elastic. Again, it is important to note that had the wall overstrength factors not been considered in the elastic analysis and design, this global behavior would not have been achieved. Equally notable is that the base wall piers in

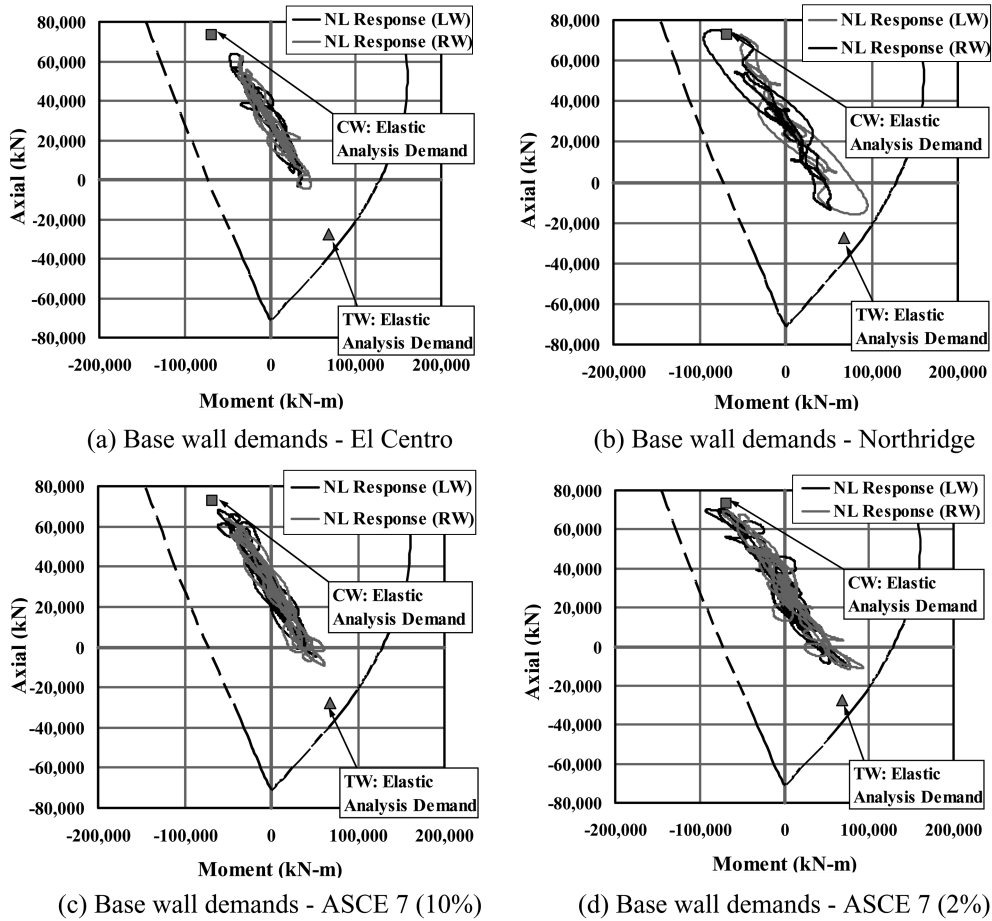


Fig. 13 Trace of base wall pier demand history for the DCB building. CW and TW are abbreviations for compression wall and tension wall, respectively. NL Response is trace of wall pier nonlinear response. (LW) and (RW) are abbreviations for Left Wall and Right Wall, respectively as shown in Fig. 1.

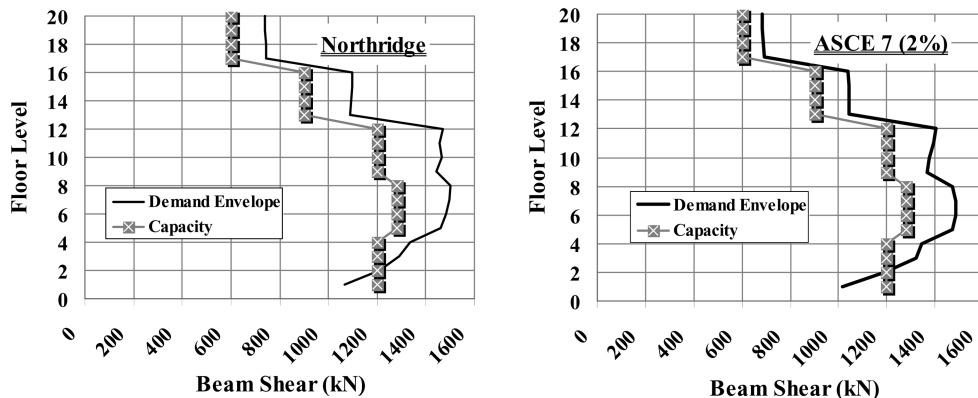


Fig. 14 Coupling beam shear demands at first yield in base wall piers

the SCB building yielded during the two more severe ground records while no wall pier yielding occurred during any of the four ground motions in the DCB building. This can be attributed to the difference in the shear strength reduction factors for steel (0.9) and diagonally reinforced concrete coupling (0.75) beams. The shear strength reduction factors contribute to the difference between the nominal shear strength of a beam and the factored shear demand; the larger the strength reduction factor, the larger the difference. Since the wall overstrength factor is a function of the nominal shear strength capacities of the beams, the wall overstrength factors are larger for larger strength reductions. This directly results in larger wall overstrength factors for wall piers in DCB buildings relative to buildings with SCB's. Consequently, wall piers in DCB buildings tend to be more heavily reinforced than wall piers in SCB buildings. In the case of the two buildings presented in this paper, the wall overstrength factor for the wall piers in the DCB building was 2.12 compared to only 1.62 for the wall piers in the SCB building. This difference resulted in significantly larger load-carrying capacities for the wall piers in the DCB building which explains the lack of wall pier yielding of the wall piers in the DCB building.

It should be noted that wall overstrength factors can be reduced if redistribution of beam shear is permitted - as is the case in Canadian practice (CSA 2004) where vertical redistribution between beams is permitted (up to 20%), provided the sum of the beam shear capacities exceeds the sum of the factored beam shears (i.e. $\sum V_n / \sum V_f \geq 1$). A good discussion of the effects of coupling beam shear redistribution is given in Harries and McNiece (2006).

5.4 Drift and coupling beam chord rotation

As can be seen in Fig. 15, the interstory and roof drifts did not exceed the code limit of 2% during any of the four ground motions. The overall lateral stiffness of the SCB building is slightly better than that of the DCB building as can be seen in Figs. 15(c) and 15(d). However, Figs. 15(a) and 15(b) suggest that steel coupling beam offers a remarkably better control of interstory drift relative to diagonally reinforced coupling beam. This is an important observation in that the expected chord rotation of a coupling beam is a critical parameter to consider during design. The performance of a coupling beam is dependent on the maximum expected chord rotation. The steel coupling beam modeled in this reported analysis shows stable hysteretic response with no strength degradation up to 36 mm (refer to Fig. 4a) of relative beam end translation which represents 4% chord rotation. Additionally, Fortney (2006(a)) reported no observed beam damage up to this point. However, referring back to Fig. 4(b), the strength of the DCB begins to degrade at about 3% chord rotation (27 mm relative beam end translation). Furthermore, Fortney (2006(b)) reported that the core of the beam degraded significantly at chord rotations beyond 3%. Referring to Fig. 15(b), the largest interstory drift in the DCB building occurred at the top floor during the Northridge ground motion and was 48 mm. This corresponds to a 2.6% chord rotation ($\delta_i/h_w = 48 \text{ mm} / 1829 \text{ mm} = 0.026$). Thus, it can reasonably be estimated that the Northridge and ASCE 7 (2%) ground motions caused severe coupling beam damage in the DCB building.

6. Conclusions

An acceptable coupled core wall system design can be achieved if appropriate design measures are taken into account. Of utmost importance is that the nominal shear capacities of the coupling beams are used to compute the wall overstrength factors. The use of wall overstrength factors ensures that the wall

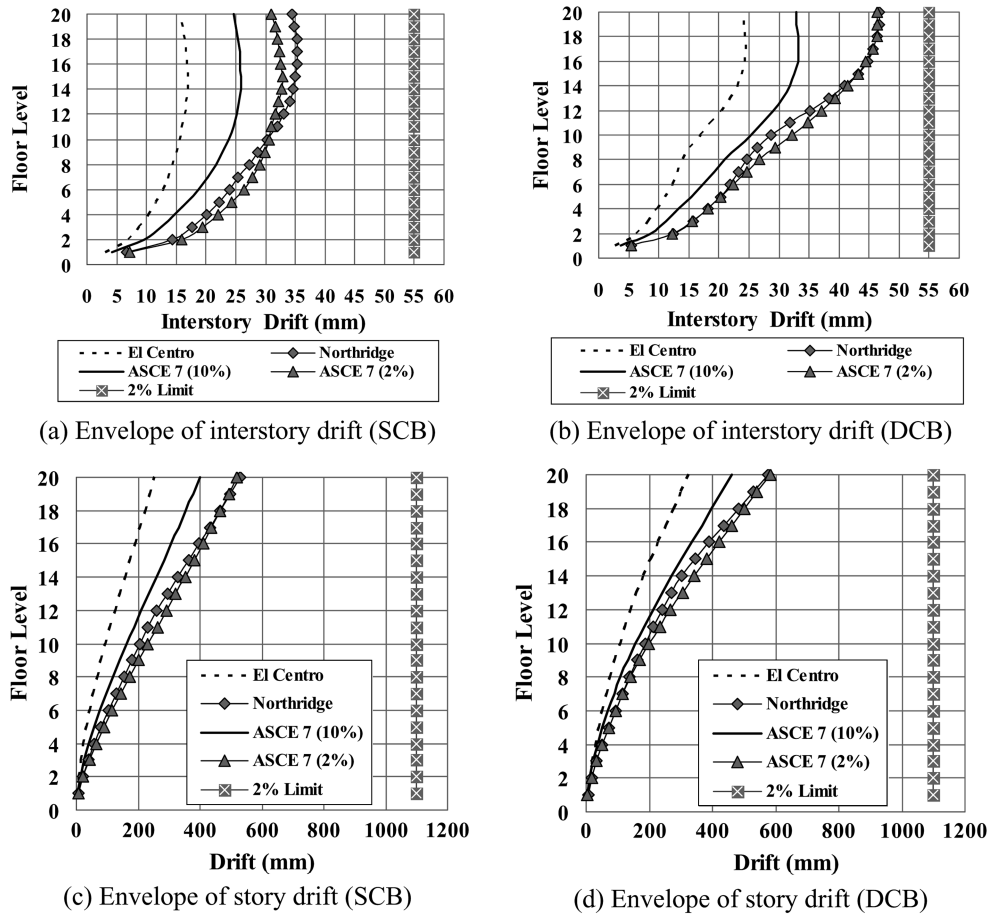


Fig. 15 Drift envelopes

piers are protected while the coupling beams go through inelastic deformations. However, wall overstrength factors can significantly increase the wall pier design loads. Consequently, the type of coupling beam used and its associated strength reduction factor, and the distribution of beam shear strength over the height of the building, must be considered.

Steel coupling beams outperform diagonally reinforced concrete coupling beams in strength, stiffness, and energy dissipation, and provide significantly better control over interstory drift than do diagonally reinforced concrete coupling beams. Additionally, the use of steel coupling beams results in substantially lower wall pier design loads due to smaller strength reductions as compared to diagonally reinforced concrete beams. This advantage, of course, is only applicable if wall overstrength factors are considered in the design, which is recommended by the authors of this paper.

From a performance perspective, steel coupling beams suffer significantly less strength degradation through cycles of larger inelastic deformations than that of diagonally reinforced coupling beams. In areas of low-to-moderate seismic activity, the diagonally reinforced concrete coupling beam considered in this research is a viable and reasonable structural component. However, in areas of high seismicity, the steel coupling beam demonstrates excellent performance where the diagonally reinforced coupling beam considered in this research is not recommended.

Acknowledgements

The reported research is sponsored by the National Science Foundation under grant BCS- CMS-9714860, with Dr. Shih Chi Liu as the program director. The project reported in this paper was part of the fifth phase of US-Japan cooperative research program on composite and hybrid structures. Any opinions, findings, and conclusions or recommendations expressed in this paper are of those of the authors and do not necessarily reflect the views of the sponsors.

References

- ACI Committee 318, 2005. *ACI 318-02/ACI 318R-02 Building Code Requirements for Reinforced Concrete and Commentary*, American Concrete Institute, Farmington Hills MI
- Canadian Standards Association (CSA) (2004), CSA A23.3-04 Design of Concrete Structures, Rexdale, Canada.
- ETABS Nonlinear version 8.4.5, copyright 1984-2004. Computers and Structures, Inc. Computer Program
- FEMA-356 (2000), "Prestandard and Commentary for the Seismic Rehabilitation of Buildings", FEMA 356/ November 2000, Building Seismic Safety Council, Washington, D.C.
- Fortney, P. J. (2005), Dissertation: "The Next Generation of Coupling Beams", Department of Civil and Environmental Engineering at the University of Cincinnati.
- Fortney, P. J., Shahrooz, B. M. and Rassati, G. A. (2006a), "Boundary detailing of coupled core wall system wall piers", *ACI Struct.* (submitted for review)
- Fortney, P. J., Shahrooz, B. M. and Rassati, G. A., (2006b), "Large-scale testing of a replaceable steel coupling beam", *J. Struct. Eng.* (submitted for review).
- Fortney, P. J., Shahrooz, B. M. and Rassati, G. A. (2006c), "Large-scale testing of concrete coupling beams with practical span-to-depth ratios", *ACI Struct. J.* (submitted for review)
- Gong, B., Shahrooz, B. M. (2001a), "Concrete-steel composite coupling beams. I: Component testing", *J. Struct. Eng.*, 625-631.
- Gong, B., Shahrooz, B. M. (2001b), "Concrete-steel composite coupling beams. II: Subassembly testing and design verification", *J. Struct. Eng.*, 632-638.
- Harries, K. A., Mitchell, D., Cook, W. D. and Redwood, R. G. (1993), "Seismic response of steel beams coupling concrete walls", *ASCE, J. Struct. Eng.*, **119**(12), 3611-3629.
- Harries, K. A., Cook, W. D., Mitchell, D. and Redwood, R. G. (1995), "The use of steel beams to couple concrete walls", *Proceedings of the Seventh Canadian Conference on Earthquake Engineering*, Montreal, Canada, 509-516.
- Harries, K. A. and McNiece, D. S. (2005), "Performance-based design of high-rise coupled wall systems", *The Structural Design of Tall and Special Structures* (in press).
- Imbsen Software Systems, 2004. XTRACT – cross sectional X sTRuctural Analysis of ComponenTs v2.6.0. Computer Program.
- Paulay, T. and Binney, J. R. (1974), "Diagonally reinforced concrete beams for shear walls", *ACI Special Publications SP 42 – Shear in Reinforced Concrete*, 579-598.
- Paulay, T. (1971), "Coupling beams of reinforced concrete shear walls", *ASCE, J. Struct. Div.*, **97**(ST 3), 843-862.
- Paulay, T. and Priestley, M. J. N. (1992), *Seismic Design of Reinforced Concrete and Masonry Buildings*, Wiley Interscience.
- Ruaumoko Nonlinear Analysis version 2.6, copyright March 2000. University of Canterbury, Department of Civil Engineering. Computer Program.
- Shahrooz, B. M., Remmetter, M. E. and Qin, F. (1992), "Seismic response of composite coupled structural walls", *Proceedings of the International Conference on Concrete*, 465-481.
- Shahrooz, B. M., Remmetter, M. E. and Qin, F. (1993), "Seismic design and performance of composite coupled walls", *ASCE, J. Struct. Div.*, **119**(11), 2858-2896.

List of symbols

b_f	: width of flange
b_w	: width of beam cross-section
d	: total depth of beam cross-section
d_h	: height of diagonal bar group (measured out-to-out of diagonal bar group transverse steel)
d_w	: width of diagonal bar group (measured out-to-out of diagonal bar group transverse steel)
E_c	: concrete modulus of elasticity
$F_y^{(+)}$: coupling beam yield strength when loading is positive
$F_y^{(-)}$: coupling beam yield strength when loading is negative
f_c^c	: specified concrete compressive strength
f_y^c	: specified steel tensile strength
h_w	: height of web from bottom of top flange to top of bottom flange -or- height of wall for which δ_i is considered
I_e	: effective moment of inertia
$I_y(TW), I_y(CW)$: moment of inertia about the y-axis for tension wall (TW), compression wall (CW)
$I_{y,avg}$: the average moment of inertia of the tension and compression walls
L	: distance between the wall pier centroids
M_T	: total overturning moment at the base of the wall piers (not including wall overstrength factor)
$M_y(TW), M_y(CW)$: moment about the y-axis causing first yield in tension wall (TW), compression wall (CW)
S_s	: mapped spectral response acceleration at short periods
S_l	: mapped spectral response acceleration at 1-second period
t_f	: thickness of flange
t_w	: thickness of web -or- thickness of wall pier
V_u	: factored shear demand
ΣV_n	: sum of the coupling beam nominal shear capacities
δ_i	: design story displacement at level being considered
ρ	: ratio of total area of reinforcement to gross area of concrete containing reinforcement
$\phi_y(TW), \phi_y(CW)$: curvature at first yield in tension wall (TW), compression wall (CW)
ϕV_n	: design shear strength

CC